Joint Stone Segmentation and Feature Driven Deformation Analysis at Water Dams

Annika Tobies[1], Judith Foth[1], André Cornelißen[1], Eike Koller[1], Lasse Klingbeil[1], Heiner Kuhlmann[1]

[1] Institute of Geodesy and Geoinformation, University of Bonn, Germany – atobies@uni-bonn.de

Keywords: Dam deformation, Terrestrial Laser Scanning, Aerial Laser Scanning, Iterative Closest Point, Stone detection

Abstract

Structural health monitoring of water dams is crucial to ensure their long-term safety and operational reliability. Traditional geodetic techniques, although precise, are limited to sparse observation points and cannot capture spatially heterogeneous deformations. Laser scanning enables comprehensive, area-wide acquisition, overcoming this limitation. Subsequent deformation analysis often relies on comparisons along the local surface normal, which are limited in detecting in-plane movements. To address this, this study presents an approach that combines image-based stone segmentation with point-cloud-based deformation analysis to estimate both in-plane and out-of-plane displacements across masonry dam surfaces. Individual stones are detected in unmanned aerial vehicle (UAV) imagery using a deep learning segmentation model (Mask R-CNN) and subsequently projected into corresponding point clouds acquired by terrestrial laser scanning (TLS) and UAV laser scanning. By establishing consistent stone correspondences across multi-epoch point clouds via centroid-based matching and local iterative closest point (ICP) alignment, the proposed method enables deformation analysis on a stone-by-stone level. Simulated deformations were applied to TLS- and UAV-based point clouds of a dam to evaluate the method. Results demonstrate that the approach achieves sub-centimeter accuracy for the TLS and low-centimeter accuracy for the UAV point cloud, as measured by the RMSE between the estimated and true deformation. Our approach outperforms conventional model-to-model comparison methods, such as Multiscale Model to Model Cloud Comparison (M3C2), for in-plane displacements. The integration of image segmentation and geometric analysis provides a powerful framework for full-field deformation monitoring of masonry structures, supporting the detection of instabilities and improving dam safety.

1. Introduction

Water dams are among the most long-lived and safety-critical infrastructures worldwide (Wieland, 2009). They are essential components of water management systems, ensuring reliable water storage and regulation for energy production, irrigation, and supply, and thereby supporting both social and economic stability (Schmitt and Rosa, 2024). However, aging structures, environmental influences, and continuous loading processes inevitably lead to deformations that may compromise structural integrity (Adamo et al., 2020). A potential failure could have catastrophic consequences for human life, infrastructure, and the environment (Wang and Wu, 2024). Therefore, continuous and reliable deformation monitoring is essential to ensure safe operation of these structures (Adamo et al., 2020).

The deformation of water dams is influenced by factors such as temperature changes, material properties, environmental conditions, and interactions with the foundation (Scaioni et al., 2018). These factors jointly produce complex displacements and strains in all three spatial directions: transverse (upstream/downstream), longitudinal (along the dam axis), and vertical (Ning et al., 2024). Hydrostatic loading and thermal gradients primarily cause downstream displacements and cyclic bending, which are correlated with water level and seasonal temperature fluctuations (Scaioni et al., 2018, Hu et al., 2019). Temperature gradients and heterogeneous foundation conditions can induce axial stresses, leading to longitudinal deformations in water dams (Mirković et al., 2022). Vertical displacements are driven by the weight of the dam, water load, and foundation settlement (Scaioni et al., 2018). In practice, dam deformation is spatially non-uniform. Variations in temperature, material stiffness, hydrostatic pressure, and foundation conditions can lead to heterogeneous deformation fields with additional localized deformation zones (Scaioni et al., 2018). Recent studies using geodetic and remote-sensing techniques confirm such spatial variability (Holst et al., 2017, Li, 2020). Hence, deformation of water dams should be interpreted as a spatially variable process in which global trends coexist with localized structural responses. Because dam behavior reflects the interaction of those structural, hydraulic, and geotechnical processes, no single observation technique can fully capture all relevant deformations (Scaioni et al., 2018). Modern monitoring concepts, therefore, combine complementary sensors operating at different spatial and temporal resolutions to ensure safety. Permanently installed instrumentation, such as tiltmeters, extensometers, or inclinometers, provides continuous measurements of relative movements within the dam body and its foundation (Adamo et al., 2021, Scaioni et al., 2018). In parallel, geodetic techniques are used to observe the absolute displacement of the entire structure and its surroundings (Scaioni et al., 2018).

The geodetic system of dam monitoring is typically realized through a control network comprising total stations and GNSS receivers positioned on the crest or on reference pillars (Scaioni et al., 2018). Such measurements provide high precision but are restricted to sparse, predefined observation points (Adamo et al., 2020). Consequently, they lack the spatial continuity necessary to identify locally limited or non-linear deformations over the dam surface. In contrast, laser scanning enables a high-density, full-field acquisition of 3D point clouds with up to millimeter-level precision and without requiring physical targets (Wu et al., 2021, Liang et al., 2016). Laser scan acquisitions can be divided into terrestrial laser scanning and multi-sensor system laser scanning. These methods differ in terms of the accuracy of the acquired point clouds, the duration required for data acquisition, and the spatial distribution of point densities. TLS typically provides high-resolution, highly accurate point clouds but is limited in spatial coverage of elevated areas and requires longer acquisition times. In contrast, multi-

sensor systems, such as UAV-based platforms, enable faster and more extensive data collection, including inaccessible areas, but at lower accuracy. The choice of sensor, therefore, depends on the intended application, including the accessibility, precision requirements, and efficiency.

Due to the full-area acquisition of laser scanners, multi-epoch point clouds have become a powerful tool for detecting temporal deformation behavior (Shen et al., 2023). Changes between epochs are commonly analyzed using cloud-to-cloud (C2C), cloud-to-mesh (C2M), or M3C2 methods (Shen et al., 2023). Due to its robustness against measurement noise and inhomogeneous point densities, M3C2 is considered state-of-the-art. These methods enable the detection of surface changes at the millimeter-to-centimeter scale (Barnhart and Crosby, 2013, Shen et al., 2023). However, they are predominantly sensitive to out-of-plane displacements and movements along the normal direction (Holst et al., 2017, Yuan et al., 2023). This limitation is particularly critical in dam monitoring, where planar surfaces are dominant. Therefore, in-plane movements, such as horizontal creep along the dam face or vertical settlements, can remain undetected.

To overcome these limitations, it is essential to identify geometrically corresponding points or regions across multiple epochs of point clouds (Yang and Holst, 2025), thereby enabling consistent comparison of both in-plane and out-of-plane displacements. In this study, we introduce a stone-based segmentation approach for masonry water dams that addresses this challenge by establishing correspondences between repeated 3D acquisitions. Individual stones are first detected in RGB imagery, and their segmentation is subsequently transferred to the 3D point cloud. By identifying and matching the same stones across epochs, this method enables the analysis of deformation at a stone-by-stone level. The proposed approach is validated on a dataset of a water dam in Germany and compared with a simulated reference deformation, demonstrating its ability to detect complex deformation patterns that may be obscured by traditional sparse point-based analyses.

2. Related work

Laser scanning has become an established technique for deformation monitoring of dam structures due to its high spatial resolution and non-contact data acquisition (Alba et al., 2006, Dreier et al., 2023). Early studies mainly focused on global registration and surface differencing, whereas more recent work has emphasized the estimation of local deformation patterns and three-dimensional displacement fields (Kregar et al., 2022, Teng et al., 2022). Common comparison approaches are well-suited for detecting out-of-plane surface changes but show inherent limitations when capturing in-plane displacements (Holst et al., 2017, Yuan et al., 2023).

Segmentation-based approaches have been introduced to address this limitation by defining surface entities that can be consistently tracked over time (Yang and Schwieger, 2023). In the case of masonry dams, a common form of water dams, individual stones serve as natural geometric units that enable local deformation analysis. Stone-based segmentation is already applied mainly in facade and heritage monitoring. It offers a promising approach for establishing reliable correspondences between multi-temporal point clouds. A distinction can be made between stone instance segmentation methods for point clouds and for images.

For point-cloud-based segmentation, methods often rely on the geometry or geometry-based features (Wiedemann and Holst, 2023, Valero et al., 2018). These approaches are well-suited to masonry with clearly defined joints and regular stone geometry. However, in rubble masonry, the absence of distinct joint depths and the irregularity of stone shapes preclude reliable separation based solely on geometric features. Alternative approaches exploit variations in intensity values between stones and joints (Dreier et al., 2025, Nespeca et al., 2024). For instance, Dreier et al. (2025) presented an instance segmentation method that leverages intensity-based features to distinguish individual stones and joints. Additionally, they show a potential for both in-plane and out-of-plane deformation analysis as an outlook. However, the reflected intensity is strongly affected by surface properties such as the type of building material, biological growth, and surface moisture, which can vary considerably across acquisition times and dam structures. As a result, the intensity contrast between stones and joints can diminish, making it impossible to reliably separate them based on intensity. In summary, methods that rely solely on geometric or intensity information tend to perform inconsistently under changing surface conditions or different masonry water dams.

Alternative methods for stone segmentation rely on image-based processing, with neural network-based approaches showing particularly strong performance (Idjaton et al., 2021, Vandenabeele et al., 2024). These approaches typically rely on distinct color or texture contrasts between stones and joints and have been evaluated mainly on datasets of historical, relatively regular masonry structures. Nevertheless, recent results suggest that extending such methods to more complex and heterogeneous stone types is promising.

Therefore, integrating image and point cloud data by combining the radiometric richness of images with the geometric precision of laser scanning offers a compelling approach to improve segmentation performance. Although several studies have already explored the adaptation of image-based segmentation techniques to point clouds (Zhang et al., 2018, Zhou et al., 2025, Yang et al., 2025), their application to the deformation analysis of dam surfaces has not yet been investigated. Building upon these ideas, our approach combines image-derived stone segmentation point clouds acquired via laser scanning with a stone-wise ICP to quantify both in-plane and out-of-plane displacements at global and local scales. This allows for a more detailed and comprehensive characterization of the deformation behavior.

3. Materials and methods

3.1 Study area and data sets

The gravity dam investigated in this study is the Brucher Dam, a masonry structure built from rubble stones with a height of 27.7 m and a crest length of 200 m (Figure 1). It is located in Marienheide in Germany. Data acquisition was carried out using three complementary datasets: Terrestrial laser scanning, UAV-based laser scanning, and UAV imagery.

The TLS data were captured using a Leica ScanStation P50 from several scan positions, with a resolution of 3.1 mm at a distance of 10 m. The individual scans were registered using reflective targets and transformed into a local dam coordinate system, as shown in Figure 2. This resulted in an average point spacing of approximately 5 mm within the water dam area.

UAV-based laser scanning was conducted using a DJI Matrice 600 Pro platform in combination with a RIEGL miniVUX-SYS laser scanner. The UAV operated at a flight speed of 0.5 m/s, resulting in an average point spacing of approximately 9 mm

Figure 1. Study area: Brucher waterdam.

for the point cloud. Further details on the acquisition setup are provided in Dreier et al. (2023).

Figure 2. TLS point cloud.

To align the UAV-derived point cloud with the TLS reference frame, six ground control points (GCPs) defined in the dam's local coordinate system were used.
The optical imagery was captured using a DJI Mini 3 Pro UAV equipped with a 1/1.3” CMOS sensor (12 MP, 24 mm equivalent focal length). The images were acquired at a manual flight with a flight distance of approximately 15 m to the water dam, resulting in a ground sampling distance of 0.5 cm/pixel. A total of 78 images were collected. The data were georeferenced using a Structure-from-Motion (SfM) approach in Agisoft Metashape (Agisoft LLC, 2024), incorporating the same six GCPs. From this image set, three images were manually annotated for training and evaluation of the image segmentation method, yielding approximately 18,000 stone instances in total.

3.2 Method

To quantify dam deformations in all three spatial directions, both locally and globally, corresponding surface regions must be identified in the respective point clouds. These regions are then matched between two observation epochs to determine the displacement field. These correspondences provide the basis for the subsequent estimation of local deformations. In this study, the individual stones of the dam surface are treated as these regions. The proposed method consists of four main steps and is schematically illustrated in Figure 3.
First, the stone instances are initially detected in the images using a deep learning-based instance segmentation approach. The detected instances are then projected into the corresponding point cloud. Multiple image acquisitions of the same stones are exploited to refine and enhance the segmentation quality in the point clouds. Based on the segmented stones identified in the two temporally separated point cloud epochs, corresponding instances are matched using a centroid-based approach. For each matched pair, the corresponding three-dimensional points of the two stones and the region around them are aligned using the ICP algorithm. This enables estimation of the local deformation of each stone. This procedure is then repeated for all stone pairs identified as matches across the dam surface. All steps of the proposed method are described in detail in the following sections.

Firstly, a deep learning-based instance segmentation approach was employed to segment individual stones on the dam surface. Specifically, a Mask R-CNN architecture (He et al., 2017) was used, which represents a state-of-the-art framework for instance segmentation (Hafiz and Bhat, 2020). It enables simultaneous detection, classification, and pixel-wise segmentation of stone instances within an image.
The image segmentation produces instance-labeled stone regions in each image $(I_1, ..., I_n)$. To obtain corresponding regions in 3D for the deformation analysis, these instance labels are transferred to the point cloud (Figure 4). For this, each 3D point (X, Y, Z) is initially projected into the image domain using the camera pose parameters $\mathbf{R}$ and $\mathbf{t}$, as shown

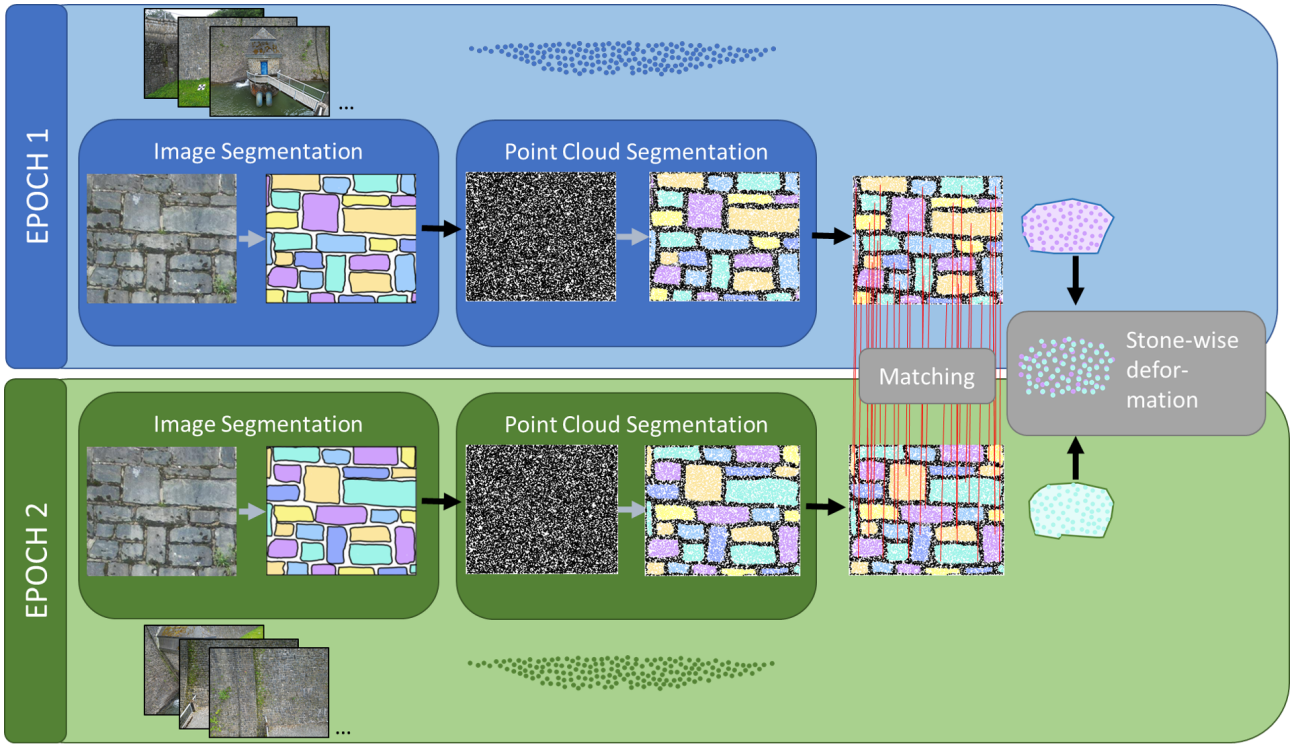

Figure 3. Overview of proposed method.

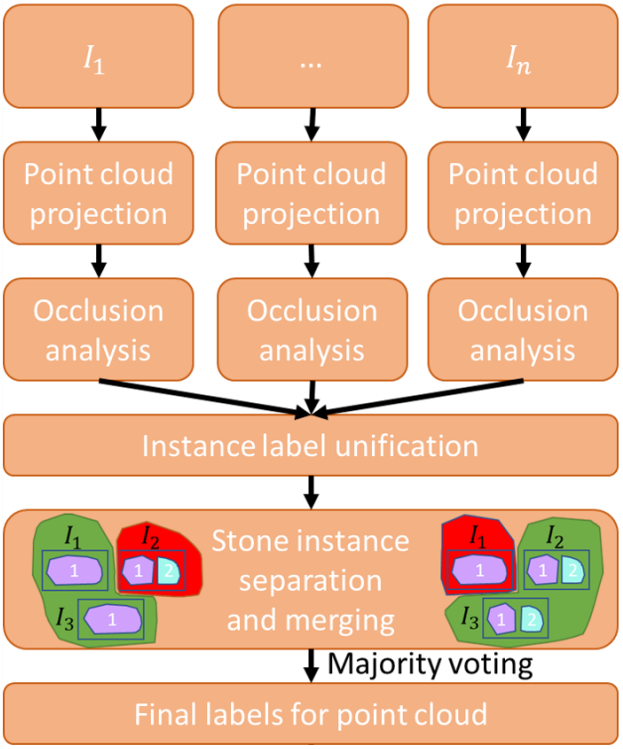

Figure 4. Point cloud segmentation.

in Equation 1 (Palaniappan et al., 2016). The intrinsic matrix $\mathbf{K}$ encodes the camera's internal parameters, including focal length and principal point, and ensures the correct transformation from camera coordinates to pixel coordinates. The instance label of the intersected pixel $[u, v]$ is then assigned to the corresponding 3D point.

$$\underbrace{\begin{bmatrix} u \\ v \\ 1 \end{bmatrix}}_{3\times1} = \underbrace{\mathbf{K}}_{3\times3} \underbrace{\begin{bmatrix} \mathbf{R} & \mathbf{t} \end{bmatrix}}_{3\times4} \underbrace{\begin{bmatrix} X \\ Y \\ Z \\ 1 \end{bmatrix}}_{4\times1} \tag{1}$$

Due to occlusions, such as the building located in the central part of the dam (Figure 1), not all points along the viewing ray are actually visible in the images. Due to gaps within the point cloud, a splatting technique is applied to generate the depth map, where each point distributes its depth value over several neighboring pixels to obtain a continuous surface representation. As a result, each 3D point is assigned a label for each image, indicating whether it belongs to a segmented instance, the background, or is not visible.
Because the same stone can be visible in different images, instance labels must be globally aligned across all images so that identical stones share a consistent label throughout the dataset. To achieve this global consistency, the Hungarian algorithm (Kuhn, 1955) is applied based on the Intersection over Union (IoU) metric between overlapping segmentation instances.

The images used for segmentation differ in terms of illumination, distance, and camera orientation. Consequently, segmentation results for individual stones vary across images, leading to merged or fragmented instances. To address this issue, we leveraged the fact that each stone is visible in multiple images and established consistent instance labeling of merged or split stones by majority voting across all available segmentations.
After generating epoch-wise consistent stone instances, the final label for each point in the point cloud can be determined. To achieve this, all available images and resulting segmentations in which the point was visible were considered. The final labels are determined by majority voting across these segmentations, assigning each point to either a specific stone instance or the background (e.g., joints).

The final result of the segmentation process is a 3D point cloud separated into stone instances. These individual stone instances are subsequently used to identify corresponding surface regions across multiple point cloud epochs, enabling both local and global deformation detection, including both in-plane and out-of-plane displacements. To achieve this, the previously independent point cloud epochs must be linked by establishing correspondences between the respective stone instances. Under the assumption that the actual deformation is smaller than the stones' characteristic dimensions (width and height), a k-nearest-neighbors (kNN) ratio-matching approach is applied based on the centroids of the stone instances. The centroid of each stone is defined as the 3D mean position of all points assigned to that instance. In the matching process, for each centroid in the reference epoch, the k nearest centroids in the comparison epoch are determined. The ratio of the distances (Equation 2) between the nearest and the second-nearest neighbors to a stone's centroid c_i is then evaluated to ensure robust correspondence, following a principle similar to Lowe's ratio test used in feature matching (Lowe, 2004).

$$\frac{\|\mathbf{c}_i - \mathbf{c}_j\|}{\|\mathbf{c}_i - \mathbf{c}_k\|} < \tau, \tag{2}$$

where

$\mathbf{c}_j$: nearest centroid to $\mathbf{c}_i$,
$\mathbf{c}_k$: second nearest centroid to $\mathbf{c}_i$,
τ : ratio threshold.

Only matches with a sufficiently low ratio are retained. Although Lowe's ratio test is known to perform best in high-dimensional feature spaces, its application to 3D centroid distances remains meaningful in this context because stones are spatially well separated. Potential ambiguities are further mitigated by enforcing consistency in surface area between matched stones. A match is retained only if the areas are sufficiently consistent.
This procedure establishes a consistent and unambiguous correspondence between epochs, providing the foundation for the deformation analysis. For each matched stone instance, the Iterative Closest Point algorithm (Plane-to-Plane correspondences) is subsequently applied to estimate the rigid transformation between epochs. For the ICP, a certain geometric variability is required. Therefore, in addition to the points belonging to the single stones, all surrounding points that lie within a predefined buffer are also incorporated.
The algorithm's parameters (ratio threshold τ, buffer around the stones, and surface-similarity ratio) were determined empirically using a 5×5 m subset of the dataset. For this purpose, a predefined grid of plausible parameter combinations was evaluated exhaustively. The optimal configuration was selected by minimizing RMSE of the computed and applied de-

formation while maximizing the number of valid correspondences. The final parameter configuration derived from the grid search is summarized in Table 1. The results further indicate that correspondence estimation is not highly sensitive to the exact choice of parameters, provided that the parameters remain within the same order of magnitude. Nevertheless, the generalizability of this parameter selection strategy to other datasets warrants investigation in future work.

Table 1. Values of the algorithm's parameters

Parameter	Value
Ratio Threshold Centroids	0.4
Ratio Threshold Surface	0.95
Buffer [cm]	60

A 60 cm buffer captures roughly one additional stone in every direction, and the joint geometry, enhancing local variability for ICP without introducing repetitive global patterns that may impair convergence.

The displacement of each stone is evaluated at its centroid c using the rigid transformation estimated by ICP. With rotation matrix $\mathbf{R}$ and translation vector $\mathbf{t}$, the three-dimensional centroid displacement d is given by

$$\mathbf{d} = (\mathbf{R} - \mathbf{I})\mathbf{c} + \mathbf{t}, \tag{3}$$

which consistently incorporates rotational effects in addition to translations. By aggregating these transformations across all matched stones, global and local displacement patterns can be derived.
This enables a continuous spatial visualization of deformations across the entire masonry water dam, providing insights into structural stability and the spatial variation of displacements over time.

4. Experiments

To evaluate the applicability of the proposed method for deformation analysis of masonry dams, we did not use two different measurement epochs. Instead, a single epoch of either the TLS or the UAV point cloud data was divided into two subsets. The original point cloud was randomly split into two disjoint point groups of approximately equal size, and the corresponding image set was divided accordingly. Each subset was processed independently to generate segmented point clouds. Splitting a single epoch of measurements enables us to simulate a two-epoch scenario using data from a single acquisition, thereby allowing a controlled evaluation independent of external influences, such as temporal variability, and facilitating comparisons with a reference deformation.

To further assess the performance of the proposed method, two types of deformations were simulated:
(1) a global in-plane deformation, implemented as a translation along the y- and z-axes, and
(2) a local out-of-plane deformation, represented by a small bulge introduced on the dam surface.

The global deformation was achieved by translating the whole point cloud 2 cm along the y-axis and 5 cm along the z-axis. The local deformation was modeled as a smooth surface bulge with a maximum depth of 5 cm and a diameter of 4 m. These deformations are applied to the second epoch of the point cloud after the segmentation. The step of applying the deformation at the point-cloud level was necessary because the images do not correspond to a deformed state of the dam.
This setup enables the evaluation of the method's applicability under both large-scale structural movements and localized surface deformations. The detected deformations were compared with results obtained using the M3C2 algorithm, a state-of-the-art method for deformation analysis in point clouds.

For evaluating stone instance segmentation, the labeled dataset was split into 90% for training and 10% for testing. The network was trained using standard hyperparameter settings from the reference implementation. No explicit hyperparameter tuning was performed, as the network serves as a preprocessing step. The trained model was subsequently applied to all images to generate consistent instance masks across the dataset.

5. Results

The results of the deformation analysis of point clouds obtained by this method depend on the segmentation accuracy of the Mask R-CNN model. After training, the neural network produced consistent results across the test instances, achieving a precision of 0.92, a recall of 0.72, an F1-score of 0.81, and a mean Intersection over Union (mIoU) of 0.84. The formulas for these evaluation parameters are, for example, provided by Naidu et al. (2023). An example of the segmentation of an image, which was not used during the training process, is shown in Figure 5. Most errors occurred at larger distances and high angles of incidence. This can be attributed to the scarcity of samples representing these conditions and the limited amount of training data. It can be expected that incorporating more diverse training data, such as from different epochs, would further improve the performance of image segmentation.

Figure 5. Example result of the stone segmentation.

Nevertheless, the segmentation quality of the stones appears to be sufficient for the subsequent analysis due to the high number of stones and the point cloud segmentation refinement achieved through various segmentations of similar stones across different images.
Based on the image segmentation results, the point cloud datasets are segmented using the corresponding image groups. A deformation is then applied to the second-epoch point cloud, after which stones from both epochs are matched to estimate individual stone translation. The two deformations (in-plane,

global translation, and out-of-plane local bump) are evaluated independently. For each of the two deformations, the proposed method determines the displacement of each stone separately for the UAV and TLS point clouds. Additionally, the deformation is also computed using the M3C2 distance and the computed normals. Since the applied deformation is known for each point or stone, the RMSE relative to this reference deformation is calculated.

In Figure 6, the result of the TLS point cloud with the applied global in-plane deformation is presented. The colors of the stones indicate the absolute distance between the matched stones of the first and second epoch. Within the point cloud, approximately $10,000$ stone matches were identified. Regions shown in gray indicate areas where no stone matches were found. The color distribution of the detected matches clearly demonstrates that the applied deformation of approximately $5.4\ cm$ is captured in most regions. Overall, stone matches are identified in most regions of the point cloud, although further improvements in the number of matched stone instances are possible, particularly through more advanced image segmentation. Fundamentally, the results confirm that the proposed method is capable of reliably detecting in-plane deformations. Only a few individual stones exhibit color values that indicate a deformation deviating from the reference. This is likely attributable to insufficient geometric variability among these stones, which causes ICP to converge to an incorrect translation. Incorporating additional geometric parameters may help prevent this issue.

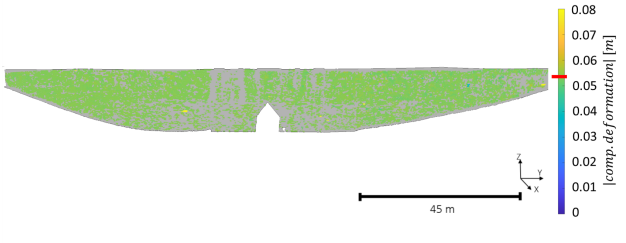

Figure 6. TLS point cloud, in plane, global deformation.

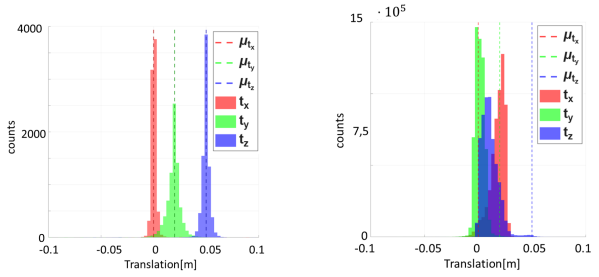

(a) (b)

Figure 7. Comparison of computed translations for the UAV point clouds: (a) segmentation-based method and (b) M3C2.

As this case represents a global transformation, the stone-wise translation parameters can also be compared globally with each other and with the reference, as shown in Figure 7. At this point, the advantages of the method for UAV-based point clouds also become evident. In contrast to the M3C2 method (Figure 7(b)), the actual translation of the segmented stones can be clearly detected (Figure 7(a)). This is also reflected by the RMSE values (Table 2), which quantify the difference between the estimated and the true deformation. For the in-plane deformation, the stone-wise results outperform the corresponding point-wise M3C2-based results for both the TLS and UAV datasets (Table 2). For both the M3C2 method and the segmentation-based approach, the TLS data yield more accurate results than the UAV data. This is likely attributable to the lower noise level in the TLS measurements. Additionally, for the segmentation-based approach, the higher noise in the UAV point clouds blurs the stone geometry, which is crucial for reliable ICP convergence.

Table 2. RMSE of detected and applied deformations.

Method	in-plane [cm]	out-of-plane [cm]
Segment.-based UAV	1.0	1.0
Segment.-based TLS	0.5	0.5
M3C2 UAV	3.2	1.3
M3C2 TLS	3.8	0.6

For the out-of-plane local bulge, a similar overall pattern is observed in the colored TLS point cloud (Figure 8). The deformation is clearly distinguishable in the global visualization, and the locally applied bulge is visually identifiable due to the continuous color gradient in the affected area. Similar to the in-plane result, a few individual stones deviate from the expected displacement pattern, and the majority of the structure consistently reflects the true deformation. A closer inspection of the bulged area in the UAV-derived point cloud indicates that the deformation exhibits a maximum vertical deviation on the order of 5 cm, which aligns well with the applied deformation parameters (Figure 9(a)). These findings demonstrate that the proposed segmentation-based approach is capable of capturing localized, out-of-plane deformations and global in-plane deformations with high spatial precision (Table 2).

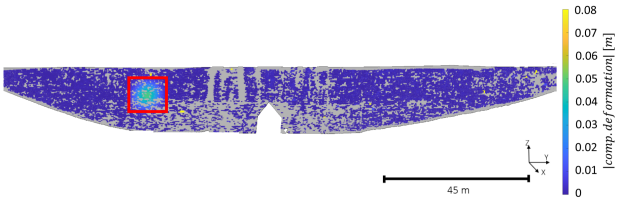

Figure 8. TLS point cloud, out-of-plane, local deformation.

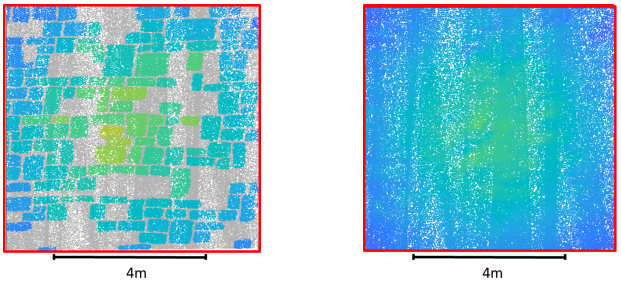

(a) (b)

Figure 9. Local out-of-plane deformation for the UAV point clouds: (a) segmentation-based and (b) M3C2.

In contrast to in-plane displacements, out-of-plane movements cause clear geometric deviations along the surface normal of the points of the water dam. Consequently, the point cloud comparison M3C2 exhibits substantially higher sensitivity and accuracy compared to those conducted in the in-plane direction

This contribution has been peer-reviewed. The double-blind peer-review was conducted on the basis of the full paper.
https://doi.org/10.5194/isprs-annals-XI-1-2026-411-2026 | © Author(s) 2026. CC BY 4.0 License.

(Figure 9 (b)). This observation is further supported by the RMSE analysis, which shows a smaller discrepancy between the estimated and the applied deformation in the out-of-plane case for the M3C2 comparison. The results for the out-of-plane deformation are, therefore, very similar for the segmentation-based and M3C2 deformation analyses. Nevertheless, the stone-segmentation method has the advantage that local stone rotations can also be extracted.

An overall comparison of the achieved RMSE values shows that the primary benefit of the proposed stone-segmentation approach lies in detecting in-plane deformations of the water dam, for which it achieves results at least twice as accurate as those obtained with M3C2. For out-of-plane deformation, the method achieves performance comparable to M3C2.
The noise characteristics of the point clouds further affect the accuracy of detectable deformation, as demonstrated by a comparison of UAV and TLS data. Deformations in TLS point clouds can be reliably detected at the sub-centimeter level, whereas UAV data allow detection only around the one-centimeter RMSE value.

Segmentation accuracy is another potential source of this uncertainty because errors can affect centroid estimation, instance matching, and ICP initialization. However, deformation estimation relies on the geometric redundancy of many 3D points within each stone and its surrounding buffer, thereby increasing robustness to moderate segmentation inaccuracies. The achieved sub-centimeter TLS accuracy and low-centimeter UAV accuracy, despite imperfect segmentation (mIoU: 0.84), indicate that segmentation quality is not the dominant source of error under the investigated conditions. A quantitative sensitivity analysis is left for future work.

6. Conclusion

In this study, we presented a novel application of neural network-based stone segmentation in images to support deformation analysis of laser-scanning point clouds of masonry dam surfaces. Individual stones were automatically identified and segmented in images, and the resulting semantic labels were subsequently transferred to the corresponding 3D point clouds. This enabled the creation of distinct and repeatable stone-based patches within the point cloud data, which served as stable geometric features across multiple observation epochs.
By establishing correspondences between these labeled stone patches, we were able to compute both in-plane and out-of-plane deformations of the dam surface between two simulated measurement epochs. The segmentation-based correspondence approach enables robust and interpretable quantification of deformations, overcoming the limitations of the state-of-the-art M3C2 method, which often fails to capture in-plane deformation components. The experiments conducted on the TLS and UAV datasets demonstrated that the proposed method effectively captures both global and local deformation patterns, including displacements of a few centimeters. Additionally, the results clearly show that TLS-based measurements yield higher accuracy and consistency than UAV-based data, primarily due to their lower noise level. Moderate segmentation inaccuracies do not prevent accurate deformation estimation because of geometric redundancy in local ICP alignment.

The presented method and the results highlight the potential of combining both image-based semantic segmentation and 3D geometric analysis to achieve a comprehensive understanding of surface behavior in complex masonry structures.
Future work will focus on improving the robustness of the proposed approach under real multi-epoch conditions and varying illumination and surface properties. Since the present evaluation was conducted using simulated deformations derived from a single acquisition epoch, the method’s transferability to real multi-epoch monitoring scenarios requires further investigation. Additionally, advances in image segmentation and the integration of image-based tracking techniques, such as correlation- or feature-based methods, will be investigated to improve the estimation of in-plane displacements. In addition, the applicability of the method will be extended to other stone and brick structures to support long-term deformation monitoring and structural health assessment.

7. Acknowledgements

This research was partly funded by the German Research Foundation (DFG) under grant number 490989047, ”Research Unit 5455 Deformation analysis based on terrestrial laser scanner measurements (TLS-Defo)”.

References

Adamo, N., Al-Ansari, N., Sissakian, V., Laue, J., Knutsson, S., 2020. Dam safety: technical problems of aging embankment dams. *Journal of Earth Sciences and Geotechnical Engineering*, 10, 281–322.

Adamo, N., Al-Ansari, N., Sissakian, V., Laue, J., Knutsson, S., 2021. Dam safety: use of instrumentation in dams. *Journal of Earth Sciences and Geotechnical Engineering*, 11(1), 145–202.

Agisoft LLC, 2024. Agisoft metashape professional, version 2.1. Software.

Alba, M., Fregonese, L., Prandi, F., Scaioni, M., Valgoi, P., 2006. Structural monitoring of a large dam by terrestrial laser scanning. *International Archives of Photogrammetry, Remote Sensing and Spatial Information Sciences*, 36.

Barnhart, T., Crosby, B., 2013. Comparing two methods of surface change detection on an evolving thermokarst using high-temporal-frequency terrestrial laser scanning, Selawik River, Alaska. *Remote Sensing*, 5, 2813–2837.

Dreier, A., Kuhlmann, H., Klingbeil, L., 2023. The potential of uav-based laser scanning for deformation monitoring. case study on a water dam. *5th Joint International Symposium on Deformation Monitoring (JISDM 2022)*, Editorial Universitat Politècnica de València, 261–269.

Dreier, A., Tobies, A., Kuhlmann, H., Klingbeil, L., 2025. Stone instance segmentation of rubble masonry based on laser scanning point clouds. *Measurement*, 242, 115905.

Hafiz, A. M., Bhat, G. M., 2020. A survey on instance segmentation: state of the art. *International Journal of Multimedia Information Retrieval*, 9(3), 171–189.

He, K., Gkioxari, G., Dollár, P., Girshick, R., 2017. Mask r-cnn. *Proceedings of the IEEE international conference on computer vision*, 2961–2969.

Holst, C., Klingbeil, L., Esser, F., Kuhlmann, H., 2017. Using point cloud comparisons for revealing deformations of natural and artificial objects. *7th international conference on engineering surveying (INGEO)*, 18–20.

Hu, Y., Shao, C., Gu, C., Meng, Z., 2019. Concrete dam displacement prediction based on an ISODATA-GMM clustering and random coefficient model. *Water*, 11(4), 714.

Idjaton, K., Desquesnes, X., Treuillet, S., Brunetaud, X., 2021. Stone-by-stone segmentation for monitoring large historical monuments using deep neural networks. *International Conference on Pattern Recognition*, 235–248.

Kregar, K., Marjetič, A., Savšek, S., 2022. TLS-detectable plane changes for deformation monitoring. *Sensors*, 22(12), 4493.

Kuhn, H. W., 1955. The Hungarian method for the assignment problem. *Naval Research Logistics Quarterly*, 2(1-2), 83–97.

Li, Y., 2020. Deformation behaviour of a concrete gravity dam based on monitoring data and numerical simulation. PhD thesis, Technische Universität Clausthal, Clausthal-Zellerfeld.

Liang, X., Kankare, V., Hyyppä, J., Wang, Y., Kukko, A., Haggrén, H., Yu, X., Kaartinen, H., Jaakkola, A., Guan, F., Holopainen, M., Vastaranta, M., 2016. Terrestrial laser scanning in forest inventories. *ISPRS Journal of Photogrammetry and Remote Sensing*, 115, 63–77.

Lowe, D. G., 2004. Distinctive image features from scale-invariant keypoints. *International Journal of Computer Vision*, 60(2), 91–110.

Mirković, U., Kuzmanović, V., Todorović, G., 2022. Long-Term Thermal Stress Analysis and Optimization of Contraction Joint Distance of Concrete Gravity Dams. *Applied Sciences*, 12(16), 8163.

Naidu, G., Zuva, T., Sibanda, E. M., 2023. A review of evaluation metrics in machine learning algorithms. *Computer Science On-line Conference*, 15–25.

Nespeca, R., Mariotti, C., Petetta, L., Mandriota, A., 2024. Point cloud segmentation in heritage preservation: advanced digital process for historical houses. *The International Archives of the Photogrammetry, Remote Sensing and Spatial Information Sciences*, XLVIII-2/W4-2024, 325–332.

Ning, X., Zhang, K., Jiang, N., Luo, X., Zhang, D., Peng, J., Luo, X., Zheng, Y., Guo, D., 2024. 3D deformation analysis for earth dam monitoring based on terrestrial laser scanning (TLS) and the iterative closest point (ICP) algorithm. *Frontiers in Earth Science*, 12, 1421705.

Palaniappan, K., Poostchi, M., Aliakbarpour, H., Viguier, R., Fraser, J., Bunyak, F., Basharat, A., Suddarth, S., Blasch, E., Rao, R. M., Seetharaman, G., 2016. Moving object detection for vehicle tracking in wide area motion imagery using 4d filtering. *2016 23rd International Conference on Pattern Recognition (ICPR)*, IEEE, 2830–2835.

Scaioni, M., Marsella, M., Crosetto, M., Tornatore, V., Wang, J., 2018. Geodetic and remote-sensing sensors for dam deformation monitoring. *Sensors*, 18(11), 3682.

Schmitt, R. J. P., Rosa, L., 2024. Dams for hydropower and irrigation: trends, challenges, and alternatives. *Renewable and Sustainable Energy Reviews*, 199, 114439.

Shen, N., Wang, B., Ma, H., Zhao, X., Zhou, Y., Zhang, Z., Xu, J., 2023. A review of terrestrial laser scanning (TLS)-based technologies for deformation monitoring in engineering. *Measurement*, 223, 113684.

Teng, J., Shi, Y., Wang, H., Wu, J., 2022. Review on the research and applications of TLS in ground surface and constructions deformation monitoring. *Sensors*, 22(23), 9179.

Valero, E., Bosché, F., Forster, A., 2018. Automatic segmentation of 3D point clouds of rubble masonry walls and its application to building surveying, repair and maintenance. *Automation in Construction*, 96, 29–39.

Vandenabeele, L., Loverdos, D., Pfister, M., Sarhosis, V., 2024. Deep learning for the segmentation of large-scale surveys of historic masonry: a new tool for building archaeology applied at the Basilica of St Anthony in Padua. *International Journal of Architectural Heritage*, 18(11), 1749–1761.

Wang, M., Wu, Z., 2024. A methodology for deformation monitoring of concrete dams based on approximate Bayesian computation with sequential Monte Carlo. *Expert Systems with Applications*, 255, 124829.

Wiedemann, W., Holst, C., 2023. Identifying individual rocks within laser scans for a rigorous deformation analysis of water dams. *5th Joint International Symposium on Deformation Monitoring (JISDM 2022)*, 327–334.

Wieland, M., 2009. Safety and lifespan of critical infrastructure projects with large damage potential: large dams. *IABSE Symposium Report*, 96, 16–21.

Wu, C., Yuan, Y., Tang, Y., Tian, B., 2021. Application of terrestrial laser scanning (TLS) in the architecture, engineering and construction (AEC) industry. *Sensors*, 22(1), 265.

Yang, X., Du, R., Huang, H., Xie, J., Xie, P., Fang, L., Guo, Z., Jiang, N., Jiang, Y., Cen, H., 2025. PlantSegNeRF: A few-shot, cross-species method for plant 3D instance point cloud reconstruction via joint-channel NeRF with multi-view image instance matching. *Artificial Intelligence in Agriculture*.

Yang, Y., Holst, C., 2025. How to Find Geometric Changes in Laser Scanning Point Clouds? A Perspective on Correspondence Definitions. *ISPRS Annals of the Photogrammetry, Remote Sensing and Spatial Information Sciences*, 1003–1010.

Yang, Y., Schwieger, V., 2023. Patch-based M3C2: towards lower-uncertainty and higher-resolution deformation analysis of 3D point clouds. *International Journal of Applied Earth Observation and Geoinformation*, 125, 103535.

Yuan, Y., Ge, Z., Lai, B., Guo, X., Zhang, Y., Liu, X., Suo, T., Yu, Q., 2023. Three-dimensional deformation measurement method based on image-guided point cloud registration. *Optics and Lasers in Engineering*, 161, 107399.

Zhang, R., Li, G., Li, M., Wang, L., 2018. Fusion of images and point clouds for the semantic segmentation of large-scale 3D scenes based on deep learning. *ISPRS Journal of Photogrammetry and Remote Sensing*, 143, 85–96.

Zhou, F., He, H., Chen, T., Zhang, T., Yang, M., Yuan, Y., Liu, J., 2025. Semantic-aware cross-modal transfer for UAV-LiDAR individual tree segmentation. *Remote Sensing*, 17(16), 2805.